



**AFRL-RZ-WP-TP-2008-2039**

**FLAME CHARACTERISTICS AND FUEL ENTRAINMENT  
INSIDE A CAVITY FLAME HOLDER IN A SCRAMJET  
COMBUSTOR (POSTPRINT)**

**Kuo-Chen Lin, Chung-Jen Tam, Isaac Boxx, Campbell Carter, Kevin Jackson, and  
Martin Lindsey**

**Propulsion Sciences Branch  
Aerospace Propulsion Division**

**FEBRUARY 2008  
Interim Report**

**Approved for public release; distribution unlimited.**

*See additional restrictions described on inside pages*

**STINFO COPY**

**©2007 AIAA**

**AIR FORCE RESEARCH LABORATORY  
PROPULSION DIRECTORATE  
WRIGHT-PATTERSON AIR FORCE BASE, OH 45433-7251  
AIR FORCE MATERIEL COMMAND  
UNITED STATES AIR FORCE**

<b>REPORT DOCUMENTATION PAGE</b>				<i>Form Approved</i> OMB No. 0704-0188			
<p>The public reporting burden for this collection of information is estimated to average 1 hour per response, including the time for reviewing instructions, searching existing data sources, gathering and maintaining the data needed, and completing and reviewing the collection of information. Send comments regarding this burden estimate or any other aspect of this collection of information, including suggestions for reducing this burden, to Department of Defense, Washington Headquarters Services, Directorate for Information Operations and Reports (0704-0188), 1215 Jefferson Davis Highway, Suite 1204, Arlington, VA 22202-4302. Respondents should be aware that notwithstanding any other provision of law, no person shall be subject to any penalty for failing to comply with a collection of information if it does not display a currently valid OMB control number. <b>PLEASE DO NOT RETURN YOUR FORM TO THE ABOVE ADDRESS.</b></p>							
<b>1. REPORT DATE (DD-MM-YY)</b> February 2008		<b>2. REPORT TYPE</b> Conference Paper Postprint		<b>3. DATES COVERED (From - To)</b> 30 April 2004 – 01 June 2007			
<b>4. TITLE AND SUBTITLE</b> FLAME CHARACTERISTICS AND FUEL ENTRAINMENT INSIDE A CAVITY FLAME HOLDER IN A SCRAMJET COMBUSTOR (POSTPRINT)				<b>5a. CONTRACT NUMBER</b> IN HOUSE			
				<b>5b. GRANT NUMBER</b>			
				<b>5c. PROGRAM ELEMENT NUMBER</b> 61102F			
<b>6. AUTHOR(S)</b> Kuo-Chen Lin and Chung-Jen Tam (Taitech, Inc.) Isaac Boxx (National Research Council) Campbell Carter, Kevin Jackson, and Martin Lindsey (Propulsion Sciences Branch, Aerospace Propulsion Division (AFRL/RZAS))				<b>5d. PROJECT NUMBER</b> 2308			
				<b>5e. TASK NUMBER</b> AI			
				<b>5f. WORK UNIT NUMBER</b> 2308AI00			
<b>7. PERFORMING ORGANIZATION NAME(S) AND ADDRESS(ES)</b>  <table border="0" style="width: 100%;"> <tr> <td style="width: 50%;"> Propulsion Sciences Branch  Aerospace Propulsion Division  Air Force Research Laboratory, Propulsion Directorate  Wright-Patterson Air Force Base, OH 45433-7251  Air Force Materiel Command, United States Air Force </td> <td style="width: 50%; vertical-align: top;"> Taitech, Inc.  National Research Council </td> </tr> </table>				Propulsion Sciences Branch Aerospace Propulsion Division Air Force Research Laboratory, Propulsion Directorate Wright-Patterson Air Force Base, OH 45433-7251 Air Force Materiel Command, United States Air Force	Taitech, Inc. National Research Council	<b>8. PERFORMING ORGANIZATION REPORT NUMBER</b> AFRL-RZ-WP-TP-2008-2039	
Propulsion Sciences Branch Aerospace Propulsion Division Air Force Research Laboratory, Propulsion Directorate Wright-Patterson Air Force Base, OH 45433-7251 Air Force Materiel Command, United States Air Force	Taitech, Inc. National Research Council						
<b>9. SPONSORING/MONITORING AGENCY NAME(S) AND ADDRESS(ES)</b>  Air Force Research Laboratory Propulsion Directorate Wright-Patterson Air Force Base, OH 45433-7251 Air Force Materiel Command United States Air Force				<b>10. SPONSORING/MONITORING AGENCY ACRONYM(S)</b> AFRL/RZAS			
				<b>11. SPONSORING/MONITORING AGENCY REPORT NUMBER(S)</b> AFRL-RZ-WP-TP-2008-2039			
<b>12. DISTRIBUTION/AVAILABILITY STATEMENT</b> Approved for public release; distribution unlimited.							
<b>13. SUPPLEMENTARY NOTES</b> PAO case number AFRL/WS07-1386, 11 June 2007. ©2007 AIAA. Presented at the 43rd AIAA/ASME/SAE/ASEE Joint Propulsion Conference and Exhibit, 8-12 July 2007, Cincinnati, OH. The U.S. Government is joint author of the work and has the right to use, modify, reproduce, release, perform, display, or disclose the work. Document contains color.							
<b>14. ABSTRACT</b> Flame structures and operating limits of an ethylene-fueled recessed cavity flameholder were investigated both experimentally and numerically, using a newly developed AFRL research scram jet flowpath at Wright-Patterson Air Force Base. Flush-wall low-angled injectors were used as main fuel injectors. The recessed cavity features an array of fueling ports on the aft ramp for direct cavity fueling. The cavity operating conditions include 1) direct cavity fueling, 2) direct cavity fueling with back pressurization, and 3) fueling from main injectors with and without direct cavity fueling. With direct cavity fueling, significant variation in the shape and spatial distribution of the cavity flame was observed at various fuel flow rates with and without back pressurization. It was found that both lean ignition and blowout limits increase with the characteristic air flow rate. The lean blowout limit is decreased toward a lower value as the shock train is pushed toward upstream. With fueling from main injectors, the flame is mainly distributed within the body wall comers for the present flowpath.							
<b>15. SUBJECT TERMS</b>							
<b>16. SECURITY CLASSIFICATION OF:</b>			<b>17. LIMITATION OF ABSTRACT:</b> SAR	<b>18. NUMBER OF PAGES</b> 24	<b>19a. NAME OF RESPONSIBLE PERSON (Monitor)</b> Campbell D. Carter <b>19b. TELEPHONE NUMBER (Include Area Code)</b> (937) 255-7328		
<b>a. REPORT</b> Unclassified	<b>b. ABSTRACT</b> Unclassified	<b>c. THIS PAGE</b> Unclassified					

## Flame Characteristics and Fuel Entrainment Inside a Cavity Flame Holder in a Scramjet Combustor

Kuo-Cheng Lin,<sup>\*</sup> Chung-Jen Tam<sup>‡</sup>  
Taitech, Inc.  
Beavercreek, OH 45430

Isaac Boxx<sup>§</sup>  
National Research Council

Campbell Carter,<sup>¶</sup> Kevin Jackson,<sup>†</sup> Martin Lindsey<sup>§</sup>  
Air Force Research Laboratory/PRAS  
Wright-Patterson Air Force Base

### ABSTRACT

Flame structures and operating limits of an ethylene-fueled recessed cavity flameholder were investigated both experimentally and numerically, using a newly developed AFRL research scramjet flowpath at Wright-Patterson Air Force Base. Flush-wall low-angled injectors were used as main fuel injectors. The recessed cavity features an array of fueling ports on the aft ramp for direct cavity fueling. The cavity operating conditions include 1) direct cavity fueling, 2) direct cavity fueling with back pressurization, and 3) fueling from main injectors with and without direct cavity fueling. With direct cavity fueling, significant variation in the shape and spatial distribution of the cavity flame was observed at various fuel flow rates with and without back pressurization. It was found that both lean ignition and blowout limits increase with the characteristic air flow rate. The lean blowout limit is decreased toward a lower value as the shock train is pushed toward upstream. With fueling from main injectors, the flame is mainly distributed within the body wall corners for the present flowpath. The rich blowout limit for a cavity fueled with both main and cavity fuel is lower than for the case with cavity fuel alone, due to main fuel entrainment from the low-angle injectors. Qualitative composition analysis indicates that the gas mixture inside the cavity mainly contains combustion products and is relatively rich with main fuel only. Consequently, additional fuel injection into the cavity increases the probability of blowing out the entire flame by disabling the flame holding capability of the recessed cavity for the present flowpath and injector designs. The rich blowout limit with main fuel injection was found to increase with the body-side fuel flow rate. Merging of fuel plumes injected from upstream injectors creates an aerodynamic blockage for air entrainment into the cavity and, consequently, reduces the rich blowout limit.

### NOMENCLATURE

ER	= fuel equivalence ratio	P	= pressure
L	= cavity length	q	= dynamic pressure
M	= Mach number	W	= cavity width
$M_{\text{flight}}$	= simulated flight Mach number	x	= free stream direction
$m^*_{\text{AIR}}$	= characteristic air flow rate	$x_s$	= shock train leading edge location
$m^*_{\text{body}}$	= fuel flow rate injected from body wall	$\phi$	= fuel equivalence ratio
$m^*_{\text{pilot}}$	= cavity fuel flow rate at operating limit		

### INTRODUCTION

The current generation of hydrocarbon-fueled scramjet combustors typically requires a flame holding device in the fixed flowpath to facilitate flame ignition and stable combustion, due to the relatively long ignition delay times of hydrocarbon fuels. Among the candidate flame holders, a recessed cavity has been shown to be effective in stabilizing the flame without excessively decreasing total pressure inside a scramjet flowpath simulating flight Mach

<sup>\*</sup>Senior Research Scientist, 1430 Oak Court, Suite 301, Beavercreek, OH 45430, Associate Fellow AIAA, corresponding author, Kuo-Cheng.Lin@wpafb.af.mil

<sup>‡</sup>Senior Research Scientist, 1430 Oak Court, Suite 301, Beavercreek, OH, Associate Fellow AIAA

<sup>§</sup>Former NRC Postdoctoral Research Associate, currently at DLR Institute for Combustion Technology-Stuttgart, member AIAA

<sup>¶</sup>Aerospace Engineer, AFRL/PRAS, Associate Fellow AIAA

<sup>†</sup>Aerospace Engineer, AFRL/PRAS, Member AIAA

<sup>§</sup>Branch Chief, AFRL/PRAS, Member AIAA

numbers of 3.5 and 4.5.<sup>1</sup> In that study, fuel entrainment from the main fuel injectors through the shear layer was the only mechanism for fueling and maintaining the cavity flame. Decoupling between main fuel plumes and cavity, resulting in flame blowout, can be a concern for some operating conditions in this type of flowpath. Maintaining a stable flame inside the cavity flame holder is crucial for the successful design of a scramjet combustor. Therefore, development of a robust cavity flame holder for scramjet applications has been an active research area.<sup>2-9</sup>

Non-reacting flow fields associated with acoustically-open cavity flame holders in several geometries were systematically studied by Gruber et al.<sup>4</sup> in a supersonic flow. The importance of an aft ramp design in determining the characteristics of shear layer/aft wall interaction was identified. It was concluded that a reduction in ramp angle creates a stable flow field around the cavity with the tradeoff of an increased drag coefficient and reduced residence time within the cavity. The mixing and combustion characteristics of a ramp cavity using various direct cavity fueling schemes were later explored by the same research team, in an attempt to expand cavity operability over a wide range of flight and fueling conditions.<sup>5</sup> The proposed use of direct cavity fueling is based on the observation that the cavity operability relied on fuel entrainment from main fuel plume upstream the cavity is relatively narrow. With the assistance of advanced laser diagnostics, it was found that fueling schemes with direct injection from the cavity ramp can create a uniform fuel/air distribution for a wide range of sustained combustion within the cavity. Back pressurization to position a shock train in front of the cavity was also explored in the study. Since the shock train leading edge is believed to be fairly close to the cavity, enhanced combustion inside the cavity was observed, due to the increased effective cavity volume produced by boundary layer separation. The idea of additional air injection directly into a ramp cavity was explored by Allen et al.,<sup>6</sup> in order to further expand the cavity operability. The strategy of injecting air from the cavity ramp right beneath the cavity fueling ports was proposed and proved to be effective in leaning out the fuel-rich gas mixture inside the cavity for stable cavity operation.

Flameholding mechanisms and structures of cavity flames inside a rectangular cavity with direct fueling from aft wall and cavity floor were studied by Rasmussen et al.<sup>7,8</sup> It was found that cavity fueling port placement can affect flame holding mechanisms and greatly change flame structures. The observations show that flame is mainly distributed under the shear layer and in the aft region of the cavity volume for the cavity directly fueled from the aft ramp. With fueling from the cavity floor, a re-circulation zone is created by the fuel jet to provide a hot zone for flame ignition. The ignited flame is distributed under the shear layer. Lean and rich blowout limits of rectangular and ramp cavities fueled with ethylene and methane directly injected from the aft wall and cavity floor were also studied by Rasmussen et al.<sup>9</sup> in supersonic flows. Major conclusions of this study include better cavity performance near the lean blowout limit for injection from the aft wall and stable flame near the rich blowout limit for injection from the cavity floor. A broader range for stable cavity operation was observed when ethylene fuel was used as opposed to methane, due to its greater reactivity (relatively shorter ignition delay time and higher flame speed).

For the studies in Refs. 5-9, combustion was established within the cavity with direct cavity fueling only. Cavity flame characteristics and cavity operation limits were explored for conditions without fuel injection from main fuel injectors. Consequently, the combined effects of fuel entrainment from main fuel injectors and independent cavity fueling on cavity or even the entire combustor operation have not been extensively investigated. With fuel entrainment from main fuel plumes, aerodynamic blockage by main fuel plumes, and the presence of a pre-combustion shock train after flame ignition, cavity flame characteristics and cavity operation limits are expected to be dramatically different from those of simple cavity operation and can depend strongly on overall flowpath and injector designs. The objectives of this study are, therefore, to explore flame structures and operation limits of a newly-designed recessed cavity operated at different fueling conditions. The conditions of interest include 1) direct cavity fuel fueling only, 2) direct cavity fueling with back pressurization, and 3) fueling from low-angle main injectors with and without direct cavity fueling. Based on the favorable features described in Refs. 4-9, the present cavity design, which is an integrated part of a newly developed scramjet flowpath, features direct fueling ports on the aft ramp to provide stable cavity flames.

## **EXPERIMENTAL METHOD**

### **Test Article**

The experiment was carried out on the thrust stand inside Research Cell 18 at Wright-Patterson Air Force Base. This facility was designed for fundamental studies of supersonic reacting flows using a continuous-run direct-connect open-loop air flow supported by the Research Air Facility. The test rig consists of a natural-gas-fueled vitiator, interchangeable facility nozzle (Mach-1.8 and 2.2 currently available), modular isolator, modular combustor, and exhaust pipe, as illustrated in Fig. 1. The rig is mounted to a thrust stand capable of measuring thrust up to 2000 lbf.

A series of compressors capable of providing up to 30 lb/s of air, with total pressures and temperatures up to 750 psia and 1600 R, respectively, supply air to the facility. An exhaust system with a pressure as low as 3.5 psia lowers and maintains the backpressure for smooth starting and safe operation. Combined with currently available Mach-1.8 and 2.2 facility nozzles, the air vitiator was fine-tuned to simulate discrete flight conditions from Mach 3.5 to Mach 5 at flight dynamic pressures up to 2000 psf. The relatively low simulated flight Mach numbers represent the scramjet takeover conditions, at which dual-mode combustion takes place.

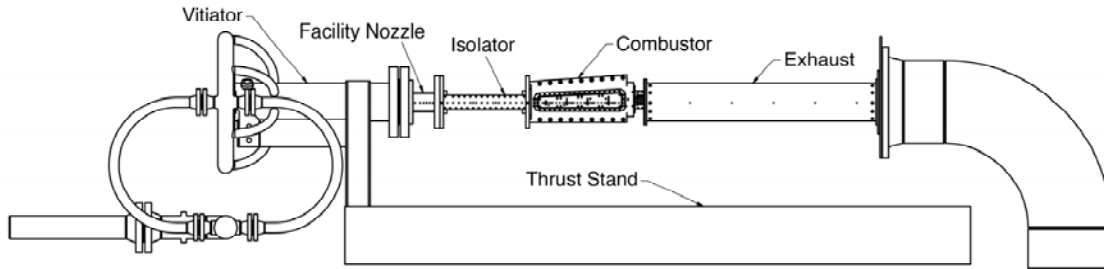


Figure 1. Schematic of Research Cell 18 combustion facility at WPAFB.

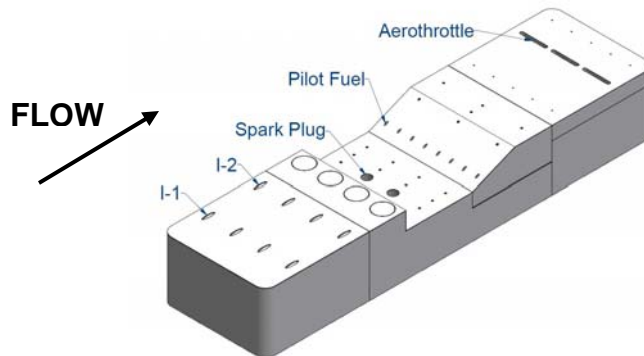


Figure 2. Integrated 3-D schematic of the injection block, cavity flame holder, and air throttle block on the body wall.

The scramjet flowpath of the present study consists of a heat-sink rectangular isolator and a rectangular combustor featuring a recessed cavity flame holder and flush-wall low-angle injectors. The isolator has a rectangular cross-section with a height of 1.5 in, a width of 4.0 in, and a length of 25.75 in. The combustor has a total length of 36 in and a constant divergence angle of 2.6 degrees. The interior surface of the entire flowpath is covered with thermal barrier coating for additional thermal protection. Two water-cooled combustor side-wall inserts can be replaced with quartz windows for flame visualization and optical measurements. The recessed cavity flame holder is located at the divergent top wall, which is designated as the body side of the scramjet-powered vehicle. A schematic of the cavity flame holder, body-side injection sites, and air throttle slots is shown in Fig. 2. This flame holder spans the entire flowpath width and has a forward-facing ramp to effectively interact with the shear layer originating from the cavity leading edge. General features of the present cavity are similar to those used in Refs. 1, 4, 5, and 9. Two conventional spark plugs, located at the base of the cavity, are used as the baseline ignition source. There are 8 cavity fuel injectors located at the cavity ramp to provide cavity fuel injection parallel to the cavity base. Four banks of injectors, two banks each on the top (body) and bottom (cowl) walls, were designed to provide various fueling options. The I-1 and I-2 injectors are upstream and downstream main fuel injectors on the body wall. The design for the gaseous fuel injectors was adopted from the study of Mathur et al.<sup>1</sup> with appropriate scaling of the orifice size. All orifices have the same diameter. Unheated ethylene was used as the fuel for both main injectors and cavity fueling ports.

### Diagnostics

#### **Basic Instrumentation**

Pressure taps and thermocouple ports were strategically positioned throughout the entire rig for instrumentation and health monitoring. The data acquisition system consists of a CAMAC-based crate (128 analog inputs, 16 analog

outputs, 48 digital inputs and 32 digital outputs channels), a 256-channel electronic pressure scanning system (Pressure Systems Incorporated) and a 64-channel thermocouple scanning system (Scanivalve Corporated). Flow rates of air, CNG, O<sub>2</sub>, ethylene, and throttling air were measured using orifice plates, sonic nozzles, venture flow meters, and turbine flow meters. Instrumentation readings were recorded directly or with preliminary reductions into a Linux based PC at 2-10 Hz frequency via fiber optic and Ethernet cable. A portable gas analyzer (Model ECOM-KL, ECOM America, Ltd.) was used to qualitatively measure dry-based gas composition sampled from the base of the cavity flame holder. The gas species of interest include O<sub>2</sub>, CO, NO, NO<sub>2</sub>, and unburned hydrocarbons. Conventional still and video cameras were utilized for flame visualization when the combustor was equipped with quartz windows.

### High-Speed Imaging

High-speed movies were acquired using a Photron FASTCAM-Ultima APX CMOS camera equipped with a 25mm diameter, fiber-coupled image-intensifier. The camera has a 10-bit, 1024×1024 pixel imaging array and is capable of full-frame image acquisition at up to 2,000 frames per second (fps). “Windowing” the array permits much higher frame rates (the exact value depends on the frame size). The combustor region was viewed through the same quartz window used for the planar laser-induced fluorescence (PLIF) measurements; in this case, the camera angle was normal to the combustion region. Depending upon run conditions, these movies were acquired at 6,000–10,000 fps, with gate times of up to 40 μs. Background-luminosity was blocked using a colored glass filter.

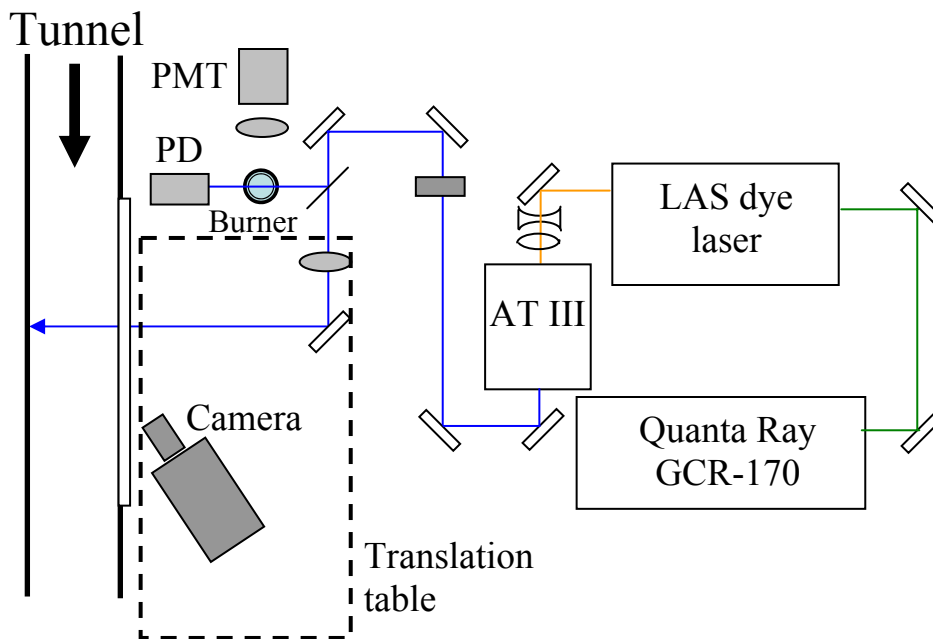


Figure 3. Optical layout for OH PLIF measurement. PMT: photomultiplier tube. PD: photodiode. AT III: the Inrad Autotracker III.

### OH-PLIF Measurement

Instantaneous measurements of the hydroxyl radical (OH) were acquired with the PLIF technique. The schematic in Fig. 3 depicts the optical layout. To generate the 283-nm radiation, a Laser Analytical Systems (LAS) dye laser was pumped with the second harmonic of an injection-seeded Spectra Physics Nd:YAG laser (GCR-170). The dye laser was tuned to 567 nm so that the frequency-doubled radiation (frequency doubling accomplished with an Inrad Autotracker III) matched the wavelength for the Q<sub>1</sub>(8) transition of the A<sup>2</sup>Σ<sup>+</sup>←X<sup>2</sup>Π (v′=1, v″=0) band. The linewidth of the 283-nm radiation was ~0.1 cm<sup>-1</sup>. To ensure good overlap of the laser and transition, a portion of the UV beam was split off and directed over a small reference flame (and then to a fast photodiode); a simple set of lenses collected and focused the resulting LIF onto the photocathode of a photomultiplier tube. This signal, along with the photodiode output, was continuously displayed on an oscilloscope, allowing minor adjustments to be made to the dye laser wavelength to mitigate the effects of ambient temperature changes.

The laser sheet was formed using a pair of fused silica lenses, a plano-concave cylindrical lens (100-mm focal length), and a plano-convex spherical lens (1000-mm focal length). This arrangement resulted in a sheet height of about 50 mm (limited by the diameter of the turning mirrors). This sheet was directed through the quartz side-window across the span of the test section and viewed off axis (normal to the sheet). Image blur was effectively mitigated by using a scheimpflug mount, similar to what is done in stereo particle image velocimetry. The transmitting and receiving optical hardware were positioned on a traversing table allowing remote positioning of the measurement volume at any streamwise location.

Although the scheimpflug mount allows the focus to be maintained across the field of view, the images still suffer from perspective distortion. The perspective distortion (which manifest itself as a variation in the magnification across the field of view) was corrected with the following procedure: first, a focusing target consisting of an array of dots was imaged; the coordinates of four corner dots of the dot-card were found; these coordinates, along with the set of ideal un-distorted coordinates, were input into a Matlab code employing the “Projective” algorithm; finally, the “de-warped” dot-card image was inspected to ensure that it matched, within reason, the undistorted dot-card. This transform was applied to all “warped” images.

A Princeton Instruments “Superblue” PIMAX intensified CCD camera ( $512 \times 512$  pixel array) was used to detect fluorescence; the pixels were binned  $3 \times 3$  before readout so that the camera could achieve a 10 frame/s readout, thus matching the laser repetition rate. The camera gate was set to 200 ns, but the fluorescence pulse is only slightly longer than the laser pulse; the interrogation time is thus about 10 ns. Typically 200 instantaneous PLIF images were acquired (and then averaged afterwards). The camera was fitted with a 105-mm f/4.5 UV lens (Nikon UV Nikkor), and Schott glass UG-5 and WG-305 filters were used to block scattering at the laser wavelength and transmit  $A \rightarrow X$  (0,0) (1,1) band fluorescence. The  $v'=0$  state is populated through vibrational energy transfer (VET), and (0,0) band fluorescence will be strong; however, (0,0) band fluorescence can be re-absorbed by OH molecules along the collection pathway (in a process called radiation trapping). The LIF images were not corrected for variation in electronic quenching or ground state population, but these should vary little in regions containing OH. The camera’s field of view extended from the side-wall window to slightly beyond the combustor mid-span.

### NUMERICAL APPROACH

The VULCAN Navier-Stokes code<sup>10,11</sup> was used to obtain the computational results in this study. VULCAN is a density-based CFD code applicable to complicated 2D and 3D geometries by using multiblock structured grids allowing for arbitrary block to block non-C(0) continuous connectivity. The code solves the Reynolds-averaged Navier Stokes (RANS) equations appropriate for calorically or thermally perfect gases with a cell-centered finite volume scheme. The equation set can be integrated in a fully elliptic or space-marched manner. The inviscid fluxes can be evaluated with central differences, Roe’s flux difference method, or a low-diffusion flux vector split scheme. Several flux limiters are provided to ensure total variation diminishing. A variety of two-equation turbulence models are available, along with one-equation and explicit algebraic Reynolds stress models. Assumed PDF options exist for modeling turbulence-chemistry interactions. Chemically reacting flows can be modeled with general finite-rate kinetics models. For parallel computation, the MPI message passing library is employed.

All calculations were performed using the low-diffusion flux split scheme of Edwards.<sup>12</sup> The MUSCL parameter  $\kappa$  was set equal to one-third to minimize truncation error and the Van Leer flux limiter was used to enforce total variation diminishing. The steady-state solutions were advanced in time using a diagonalized approximate factorization scheme. These solutions were advanced in time with either a Courant-Friedrichs-Levy number in the range of 1.0-4.0 or with a constant time step in the range of 0.2-0.5  $\mu$ s. Steady-state solutions could not be obtained for some of the simulations in this effort. When the flow was unsteady, a constant time step was employed and the flow was typically observed to be periodic. Consequently, an effective steady-state solution was obtained through an ensemble average of the flow field over one to three periods.

The Menter baseline (BSL) turbulence model<sup>13</sup> was used in this work. The Menter model is essentially the standard high-Reynolds-number form of the Wilcox  $\kappa$ - $\omega$  model near solid surfaces, but it smoothly transitions to the standard Jones-Launder  $\kappa$ - $\epsilon$  model near the outer portion of the boundary layer and in regions of free shear. The model is designed to take advantage of the accuracy and stability of the  $\kappa$ - $\omega$  formulation for wall-bounded flows, while retaining the somewhat more accurate  $\kappa$ - $\epsilon$  formulation for free shear flows. To relax the grid requirements near solid surfaces, the wall matching procedure of Wilcox was employed.<sup>14</sup>

All calculations employed constant values for the turbulent Schmidt  $Sc_T$  and Prandtl  $Pr_T$  numbers, which control the transport of mass and energy, respectively. Previous dual-mode calculations have demonstrated a strong sensitivity to the values chosen for these parameters, particularly for the Schmidt number.<sup>15,16</sup> The baseline values for the turbulent Schmidt and Prandtl numbers were set equal to 0.50 and 0.89, respectively. A study of sensitivity to the turbulent Schmidt number was performed and values in the range of  $0.20 \leq Sc_T \leq 1.0$  were considered.

Advancing from the semi-global model developed by Singh and Jachimowski,<sup>17</sup> a recently developed model, using quasi-steady state (QSS) approximations,<sup>18</sup> was employed for the simulations of ethylene-fueled supersonic combustion in the present study. This new model is referred to subsequently as the Law model. This reduced model was based on a detailed ethylene oxidation mechanism from Qin et al.<sup>19</sup> that consists of 70 species and 463 elementary reactions. First, a skeletal reduction was applied to identify and eliminate unimportant species and reactions. For the skeletal reduction, perfectly stirred reactor (PSR) and auto-ignition calculations were used over a range of conditions yielding a skeletal mechanism consisting of 33 species and 205 elementary reactions. Then a time scale reduction technique (QSS approximation) was applied. The computational singular perturbation (CSP) method was used to identify the QSS species again using PSR and auto-ignition as the data bases. A species was assumed to be a QSS species if its worst case normalized time scale was shorter than a specified threshold value. The QSS species were then removed from the skeletal mechanism and an internal algebraic loop was used to solve the concentrations of the QSS species. The final reduced mechanism consisted of 19 species or 15 global steps. These 19 species are:  $H_2$ ,  $H$ ,  $O$ ,  $O_2$ ,  $OH$ ,  $H_2O$ ,  $HO_2$ ,  $H_2O_2$ ,  $CH_3$ ,  $CH_4$ ,  $CO$ ,  $CO_2$ ,  $CH_2O$ ,  $C_2H_2$ ,  $C_2H_4$ ,  $C_2H_6$ ,  $CH_2CO$ ,  $C_3H_6$ , and  $N_2$ . The removal of the short time scales effectively reduces the stiffness of the system as well as the number of differential equations. The CPU cost per iteration of the Law model was approximately 10 times the cost of the Jachimowski 10-species global model. The Law model typically required fewer iterations to attain convergence, however, and retained significantly higher kinetics fidelity. The VULCAN code has been modified to interface these reduced models, which are not in standard Arrhenius equation form through a driver routine. The driver routine passes the static temperature, static pressure and composition to the routine containing the reduced kinetics model and returns the species production rates.

## RESULTS AND DISCUSSION

### Pure Cavity Flame

Photographs of typical cavity flames with various independent cavity fuel flow rates are shown in Fig. 4, where the simulated flight condition has a flight Mach number of 5.0 and a dynamic pressure of 1000 psf. The freestream air is from right to left in Fig. 4. The flame was ignited with two spark plugs without the aide of air throttling to create a shock train. The high-speed camera was positioned at an angle relative to the freestream to better depict the flame spatial distribution within the cavity. With the fuel flow rate around the lean ignition limit, the flame is mainly distributed above the cavity floor and beneath the shear layer, as can be seen in Fig. 4(a). As the fuel flow rates increase slightly in Fig. 4(b), the cavity flame originates from the cavity lip, along the shear layer initially, and then terminates at the foot of the cavity ramp, just in front of the cavity fueling ports. Increased fuel concentration prevents the appearance of flame within the region right behind the cavity backward-facing step as will be discussed later. As the fuel flow rate is further increased in Fig. 4(c), the flame within the shear layer disappears. The majority of the flame emission originates from a “fire ball” located at the foot of the cavity ramp. Finally, the flame is mainly distributed along the cavity ramp like a thick blanket, as the fuel flow rate approaches the rich blowout limit in Fig. 4(d). A significant portion of the cavity volume is not filled with the flame in this condition. Significant differences in flame shape and spatial distribution inside the cavity can be observed as the fuel flow rate varies, as previously noted by Rasmussen et al.<sup>7</sup>

Figure 5 shows representative instantaneous images, taken using the high-speed CMOS camera, for cavity flame fueled by independent cavity fueling ports at various operating limits. The simulated flight condition in Fig. 5 is identical to that in Fig. 4. The flame in Fig. 5(a) is created with a cavity fuel flow rate near the lean ignition limit, where fuel flow rate is the smallest possible for successful flame ignition. The appearance and distribution of the cavity flame are similar to those observed in Fig. 4(a). From this viewing angle, the flame is apparently confined right above the cavity floor and may not directly interact with the main fuel plumes for main flame ignition. Figure 5(b) shows the cavity flame operating near the rich ignition limit, where the fuel flow rate is at the highest level possible for successful flame ignition. At this cavity fuel flow rate, the flame is distributed within the initial shear layer and then bent toward the foot of the cavity ramp. Both lean and rich ignition limits were obtained while the cavity wall was relatively cold. Figure 5(c) shows the cavity flame near the rich blowout limit, where the cavity

flame can still be maintained with the maximum possible fuel flow rate. Similar to Fig. 4(d), the flame in Fig. 5(c) is mainly distributed along the ramp surface with some spillage over the cavity ramp into the main flow path.

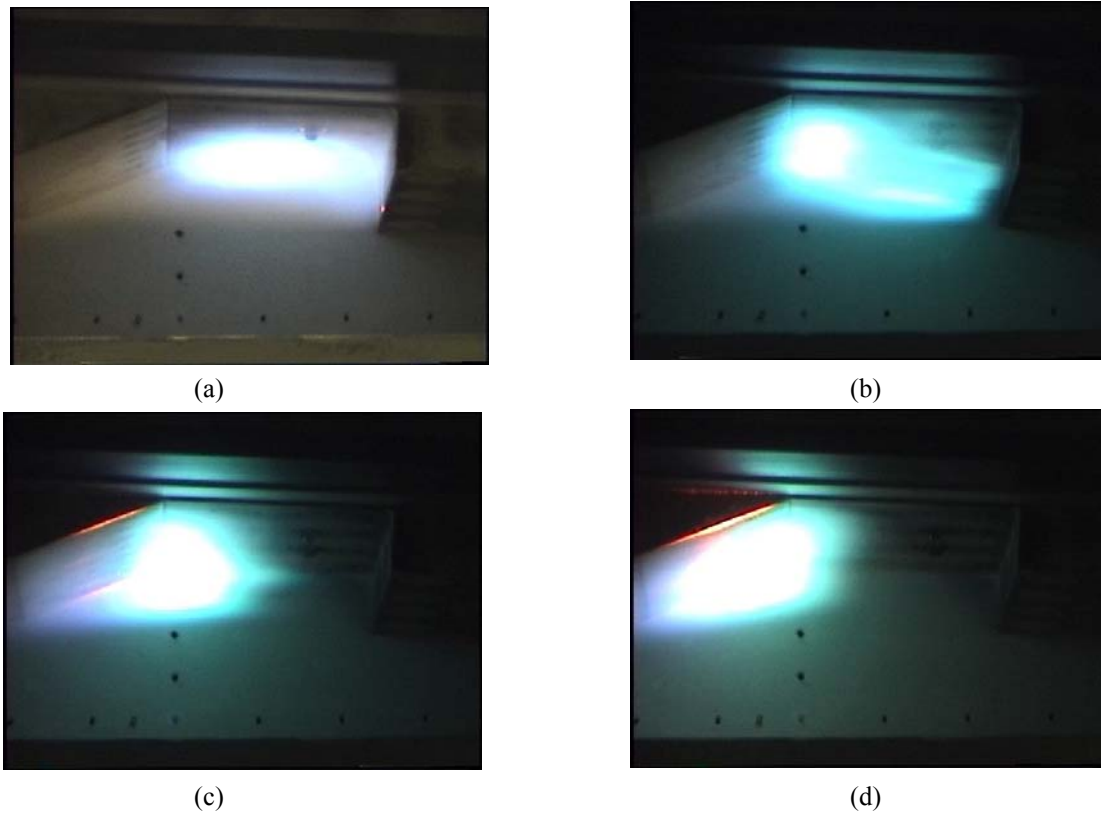


Figure 4. Photographs of cavity flames with various independent cavity fuel flow rates for  $M_{flight}=5.0$  and  $q=1000$  psf. No backpressure. (a) 0.0011 lb/s, (b) 0.0028 lb/s, (c) 0.0060 lb/s, (d) 0.0082 lb/s.

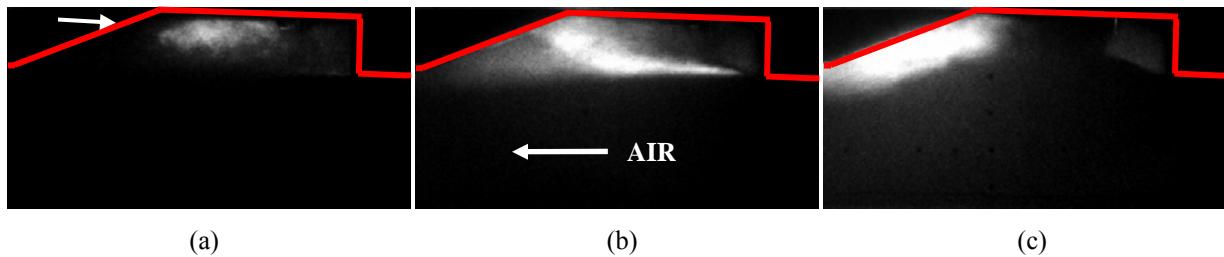


Figure 5. Instantaneous images from a high-speed video camera for cavity flames with various independent cavity fuel flow rates for  $M_{flight}=5.0$  and  $q=1000$  psf. (a) Near lean blowout limit, 0.0011 lb/s, (b) Near rich ignition limit, 0.0047 lb/s, (c) Near rich blowout limit, 0.0089 lb/s.

To explain the observed difference in flame shape and flame distribution in Figs. 4 and 5, numerical simulations of the cavity flame with independent cavity fueling from the work of Liu et al.<sup>18</sup> were utilized, with some expansions. The original objective of this work emphasized the development of a reduced chemical kinetics mechanism using cavity-stabilized flames as the validation platform. The cavity geometry is similar to the present cavity with a slightly smaller aspect ratio ( $L/D$ ). Figure 6 shows the temperature contours for a cavity operated at various cavity fuel flow rates inside a Mach 2.0 supersonic crossflow. Only a slice of the computational domain, which spans from the injector center-plane to the mid-plane between two injectors, is shown. At a fuel flow rate four times the lean blowout limit, in Fig. 6(b), the high temperature region is extended from the cavity leading edge to the cavity fueling port and is similar to the flame structure observed in Figs. 4(b) and 5(b). The corresponding fuel equivalence ratio contours in Fig. 7(b) indicate that the rich fuel/air mixture is mainly distributed at the cavity base and the cavity flame is mainly distributed around the stoichiometric line, identified as a white line in Fig. 7. As the fuel flow rate is

further increased to ten times the lean blowout limit in Fig 6(c), the high temperature region is mainly located at the ramp surface, as observed for flame distribution in Figs. 4(d) and 5(c). Flame spillage into the main flowpath behind the cavity is also depicted in Fig. 6(c). The corresponding fuel equivalence ratio contours in Fig. 7(c) show that the region containing the rich fuel/air mixture occupies the majority of the cavity volume with the flame still burning at a relatively fuel-rich condition above the cavity ramp. It can also be seen in Fig. 6(c) that there is no flame distributed around the stoichiometric line, which is pushed out of the cavity volume by the rich mixture, probably due to relatively high strain rates within the shear layer. For the cavity operated around the lean blow limit, the equivalence ratio contours in Fig. 7(a) imply that the flame should be distributed right above the cavity floor, where the combustible mixture is mainly located. Figures 4(a) and 5(a) substantiate this expectation. Further examining the numerical streamlines in Fig. 7 shows that size and structure of the major re-circulation zone inside the cavity are not affected by the cavity fuel flow issuing from the present fueling port design.

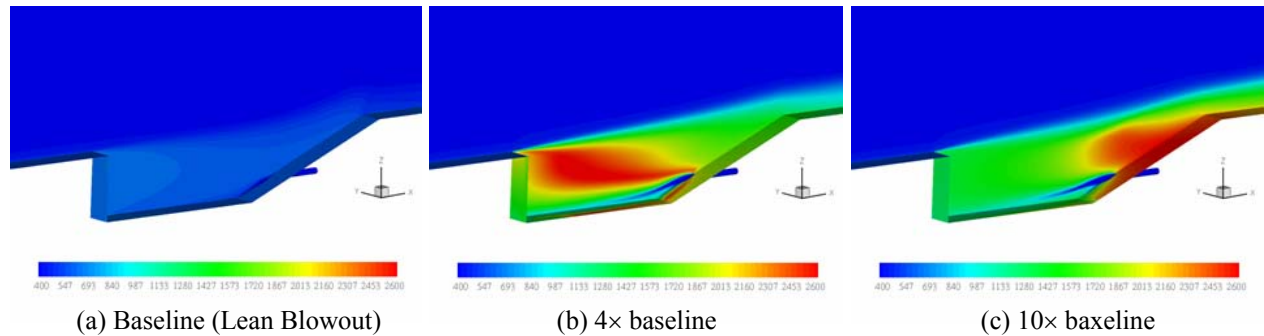


Figure 6. Temperature contours around the cavity fueled with independent cavity fuel injectors inside a Mach 2.0 crossflow environment. (a) At lean blowout limit, (b) 4 times the baseline flow rate, (c) 10 times the baseline flow rate.

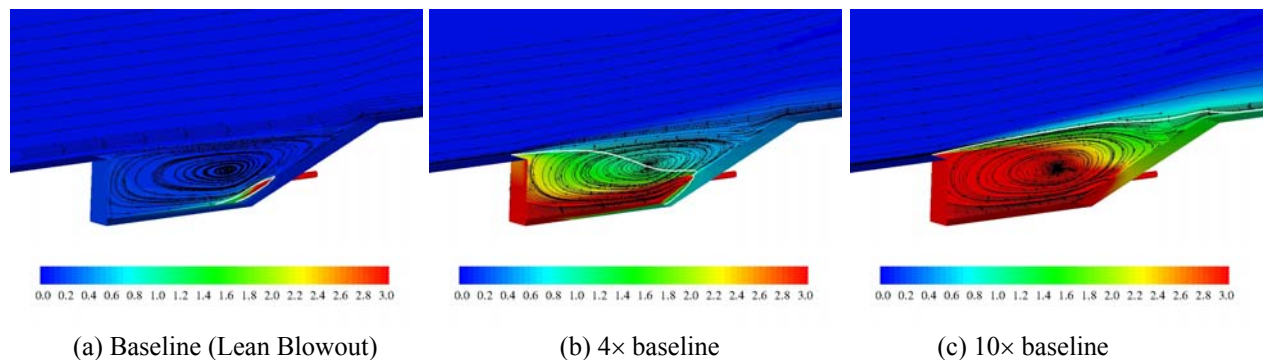


Figure 7. Equivalence ratio contours and streamlines around the cavity fueled with independent cavity fuel injectors inside a Mach 2.0 crossflow environment. The white line marks the stoichiometric condition. (a) At lean blowout limit, (b) 4 times the baseline flow rate, (c) 10 times the baseline flow rate.

Based on the observations in Figs. 4-7, the gas mixture inside the cavity fueled with independent fueling ports will never be well premixed for combustion. Instead, due to the present fueling port design, the injected fuel flow will align with the structure of the main re-circulation zone and initially fill the bottom of the cavity. Consequently, the combustion zone is mainly located near the cavity floor (Figs. 4(a) and 5(a)). As more fuel is injected into the cavity, the region with fuel-rich mixture expands gradually toward the cavity surface. The shear layer emanating from the cavity leading edge initially represents a restriction boundary for the growth of the fuel-rich region, due to its high-momentum air stream. The region with mixtures near the stoichiometric condition, therefore, stays right beneath the shear layer and extends toward the cavity ramp, where the shear layer impinges the cavity (Figs. 4(b) and 5(b)). Eventually, the fuel-rich region overcomes the high-momentum shear layer and pushes the region with mixtures near the stoichiometric condition out of the cavity volume, as more fuel is injected. No flame, however, can be established above the cavity surface, due to excessive strain rate in the freestream. Instead, the flame is mainly

distributed along the ramp surface, where the shear layer impinges to create a relatively stagnant flow region (Figs. 4(d) and 5(c)).

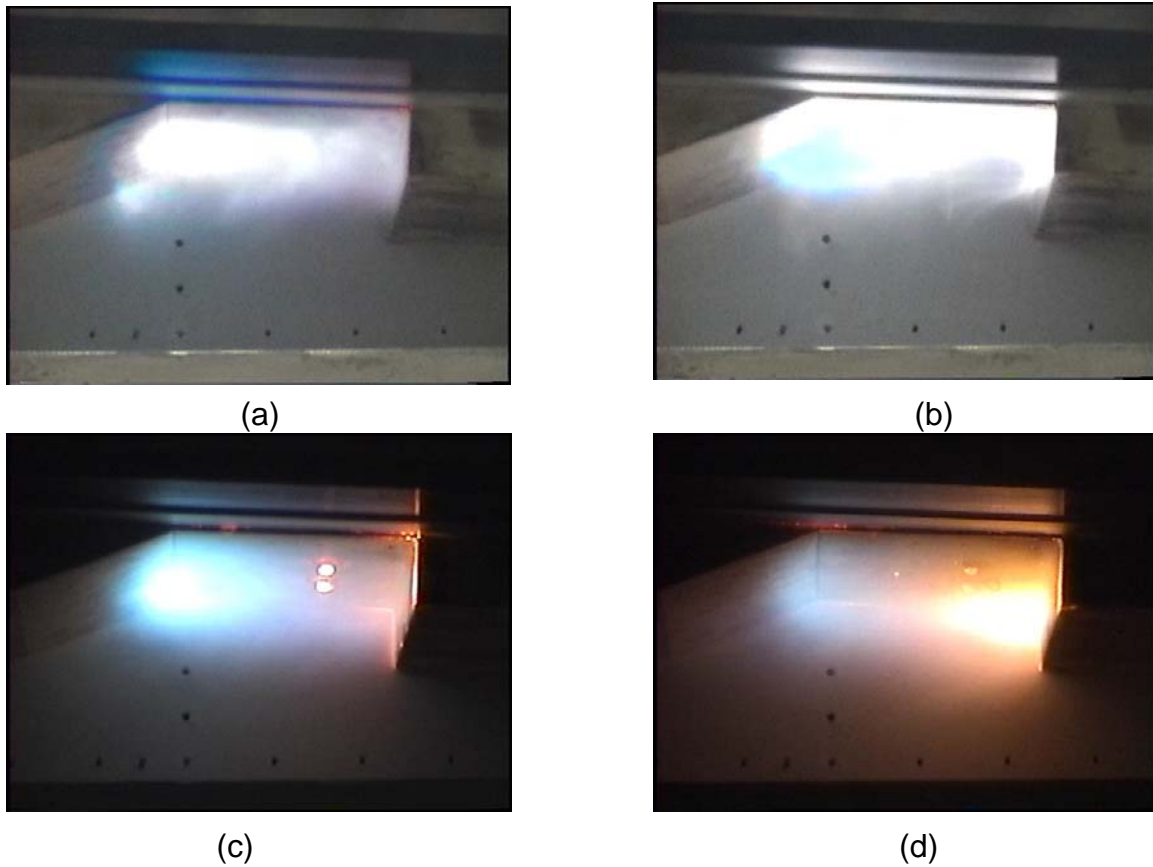


Figure 8. Photographs of cavity flames with various independent cavity fuel flow rates for  $M_{\text{flight}}=5.0$  and  $q=1000$  psf. Back pressure was applied to position the shock train at the combustor entrance. (a) 0.0017 lb/s, (b) 0.0026 lb/s, (c) 0.0068 lb/s, (d) 0.0093 lb/s.

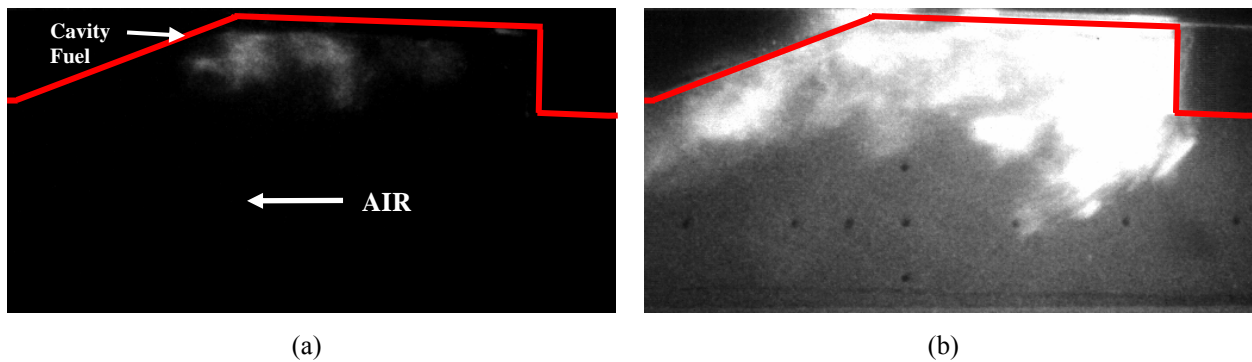


Figure 9. Instantaneous images from a high-speed video camera for cavity flames with various independent cavity fuel flow rates for  $M_{\text{flight}}=5.0$  and  $q=1000$  psf. Back pressure was applied to position the shock train at the combustor entrance. (a) Near lean ignition limit, 0.0021 lb/s, (b) Near rich blowout limit, 0.0089 lb/s.

#### Pure Cavity Flame with Backpressure

Local pressurization around the cavity region, using an air throttle located downstream of the cavity, is one of the ignition aides used to facilitate successful scramjet ignition. In addition, a pre-combustion shock train established from sustained combustion exists inside a dual-mode scramjet flowpath. Local pressurization for both conditions can significantly change the flow field around the cavity. One major difference is that the freestream Mach number

decreases from supersonic to high subsonic around the cavity region. Therefore, characteristics of the cavity flame under local pressurization should also be investigated.

Figure 8 shows photographs of cavity flames with various cavity fuel flow rates under back pressurization. A shock train was established at the entrance of the combustor, using the air throttle, before cavity flame ignition. The simulated flight condition is the same as that in Fig. 4. Due to unsteadiness of the shock train, the cavity flame appears to be highly unsteady at a low cavity fuel flow rate. The instantaneous image in Fig. 8(a) shows that the majority of the cavity is filled with the flame with a high intensity combustion zone located right above the cavity floor. With a similar cavity fuel flow rate, the shape and location of the high intensity combustion in Fig. 8(a) resemble those of the cavity flame without back pressurization in Fig. 4(a). As the fuel flow rate is slightly increased in Fig. 8(b), the cavity is filled with more unsteady high-intensity combustion. The flame structure, however, is significantly different from that in Fig. 4(b) for a similar cavity fuel flow rate. Figure 8(c) shows the cavity flame as the cavity fuel flow rate is further increased. The cavity flame structure is similar to that in Fig. 4(c), except that a region with yellow luminosity appears right behind the cavity step, probably due to continuum radiation from soot particles. The glow from two spark plugs, which were not activated for flame ignition, also comes from radiation. The blue flame in Fig. 8(c) appears dimmer when compared with the blue flame in Fig. 4(c). The cause of the appearance of yellow luminosity is unclear at this point. The yellow soot-containing flame increases its size and intensity as the cavity fuel flow is further increased in Fig. 8(d). Meanwhile, the blue flame located in front of the cavity fueling ports becomes dimmer and smaller at this high cavity fuel flow rate. A significant difference in flame structures can be easily seen between the flames with and without back pressurization in Figs. 8(d) and 4(d), respectively. Obviously, the change in freestream flow properties due to the presence of a shock train in front of the cavity can substantially change flame structures. Numerical assessment of the flame structures under back pressurization can not be completed at this time and will be performed in the future.

Figure 9 shows instantaneous images of cavity flames obtained from the high-speed video camera at two fuel flow rates under back pressurization. Like the flame in Fig. 8(a), the cavity flame in Fig. 9(a) is mainly located above the cavity floor close to the foot of the cavity ramp when the cavity fuel flow is close to the lean ignition limit. The flame structure near the rich blowout limit in Fig. 9(b) shows a significant extension of the cavity flame out of the cavity volume. As will be discussed later, the flame extending out of the cavity volume is mainly distributed along the side wall window only and does not span the freestream core flow. With a similar cavity fuel flow rate, the flame seen in Fig. 9(b) is also quite different from the flame in Fig. 8(d), probably due to the difference in camera sensor sensitivity to flame emission spectrum. Nonetheless, the combination of Figs. 8(d) and 9(b) gives a more complete picture of the cavity flame operating near the rich blowout limit under back pressurization.

### **Cavity Operating Limits for Pure Cavity Flame**

Operating limits, including the lean ignition limit (LIL), lean blowout limit (LBL), and rich ignition limit (RIL), of the present cavity geometry operating inside the present flowpath with and without back pressurization were measured at various simulated flight conditions and are tabulated in Table 1. The measurements of LIL and RIL were obtained by gradually increasing the cavity fuel flow rate from zero and decreasing the cavity fuel flow rate from the maximum flow meter capacity, respectively, until successful flame ignition in the cavity. During the fuel flow rate adjustment, the cavity wall temperature was relatively cold. The measurement of LBL was obtained by gradually reducing the cavity fuel flow rate for an ignited cavity flame until the flame was blown out. Therefore, the cavity wall temperature was elevated by the cavity flame for a certain period of time and hot combustion products were present inside the cavity before flame blowout. The measurement of rich blowout limit (RBL) for the pure cavity flame, however, was not obtained during the present study, since the RBL of the pure cavity flame was found to be beyond the flow meter capacity of the present setup.

Figure 10 shows the measured cavity operating limits at various characteristic air flow rates,  $m^*_{\text{air}}$ , which is defined as  $\rho_{\infty}u_{\infty}(WL)$  and is used to scale with the air entrainment into the cavity volume. Instead of considering actual air entrainment through the shear layer, which is difficult to quantify, the present study follows the work of Rasmussen et al.<sup>9</sup> and uses the product of cavity width (W) and cavity length (L) to represent the cavity opening area for air entrainment. The characteristic air flow rate was adjusted by varying the vitiator operating conditions using the Mach 1.8 and 2.2 nozzles. High characteristic air flow rates correspond to flight conditions with high Mach numbers and high flight dynamic pressures. As can be seen in Fig. 10, both LIL and LBL increase with the characteristic air flow rate. The measured LBL is typically lower than the LIL. Both observations agree with those of Rasmussen et al.<sup>9</sup> The difference between LBL and LIL at the same vitiator operating condition is believed to come from the

differences in gas mixture characteristics inside the cavity and the cavity wall temperature. With a hot wall and hot combustion products to preheat cavity fuel during injection and to preserve heat within the cavity volume during fuel flow rate adjustment, a lower flow rate can be achieved for LBL. Only three RILs were obtained (shown in Fig. 10), due to limited flow meter capacity. For these three conditions, the unobtainable RBL was observed to be higher than RIL, due to the presence of hot combustion products and the effect of cavity wall temperature.

Table 1 Cavity operating limits at various vitiator conditions

(a) Flight conditions simulated with the Mach 2.2 nozzle

$M_{flight}$	q (psf)	$x_s$ (in)	Spark Plug	Pilot Fuel Mass Flowrate (lb/s)			Note
				Lean Ignition Limit (LIL)	Lean Blowout Limit (LBL)	Rich Ignition Limit (RIL)	
5.0	500		2				No Ignition
5.0	500	32	0	0.0019	0.0016		Auto Ignition
5.0	500	20	0	0.0013			Auto Ignition
5.0	500	16	0	0.0010	0.0008		Auto Ignition
5.0	500	12	0	0.0010			Auto Ignition
5.0	1000		2	0.0011	0.0011	0.0047	Initial air @ 500 F
5.0	1000		2	0.0013	0.0012	0.0047	Initial air @ 70 F
5.0	1000	~ 26"	0	0.0021			Auto Ignition

(b) Flight conditions simulated with the Mach 1.8 nozzle

$M_{flight}$	q (psf)	$x_s$ (in)	Spark Plug	Pilot Fuel Mass Flowrate (lb/s)			Note
				Lean Ignition Limit (LIL)	Lean Blowout Limit (LBL)	Rich Ignition Limit (RIL)	
3.5	500		2				No Ignition
3.5	500	12	2	0.0013	0.0010		
3.5	1000		2	0.0021	0.0012	0.0041	
3.5	2000		2	0.0031	0.0021		
4.0	500		2				No Ignition
4.0	500	12	2	0.0014	0.0011		
4.0	1000		2	0.0022	0.0012	0.0043	

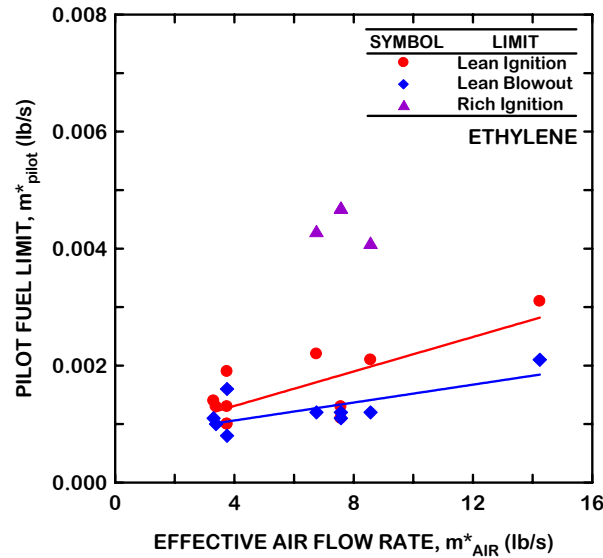


Figure 10. Cavity fuel flow rates at various cavity operating limits.

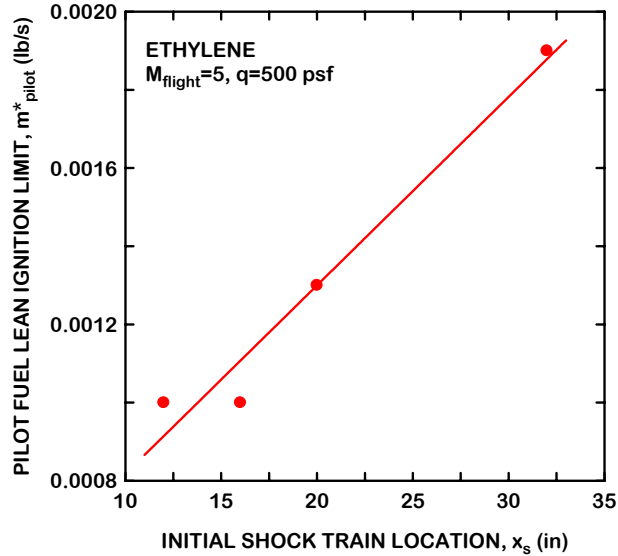


Figure 11. Cavity fuel flow rates for cavity operating at lean ignition limit with the shock train established at various locations inside the isolator before flame ignition.

The relationship between LIL and shock train location,  $x_s$ , inside the isolator is illustrated in Fig. 11. The shock train was positioned at the desired location, using air throttle to create back pressure, before introducing cavity fuel to explore LIL. For the conditions in Fig. 11, auto-ignition occurred at each LIL. For a given vitiator operating condition, a lower LIL can be obtained when the shock train is positioned further upstream, probably due to changes in air entrainment characteristics as well as local temperature and pressure. An elevation in both local temperature and pressure due to a higher level of back pressurization can significantly reduce the ignition delay time of the fuel/air mixture inside the cavity and thus LIL. For the vitiator condition in Fig. 11, the cavity flame cannot be established by spark plugs without back pressurization.

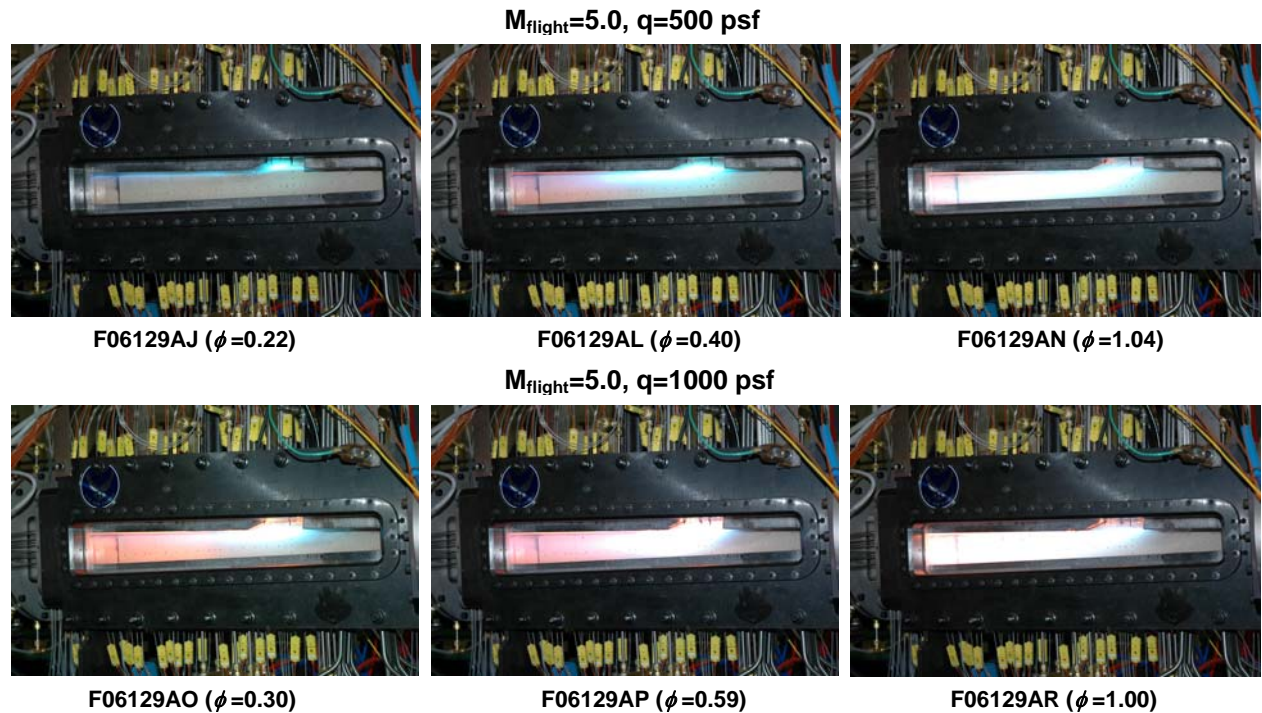


Figure 12. Photographs of the flame inside the scramjet combustor at various simulated flight conditions and fuel flow rates. Unheated ethylene was injected from the I-2 injection site.

### Cavity Flame with Main Fuel Injection

Figure 12 illustrates the flame appearance inside the scramjet combustor with ethylene injected from the I-2 injectors at various flight conditions and fuel flow rates. No independent cavity fuel was introduced for these conditions. The flow is from right to left. It appears that the flame originates from the cavity leading edge and is mainly distributed around the cavity flame holder and along the downstream body wall for the present fueling scheme. Flame luminescence, which has been reduced substantially with a fixed high-speed camera shutter, still exhibits saturation for most of the images in Fig. 12. It appears that high-intensity combustion may not fill the entire cavity volume. No images with other fueling schemes were taken due to failure of the quartz window from excessive thermal shock. Flame spreading in the spanwise direction and highly unsteady features of the flame can not be depicted from these images.

To further explore the flame structures around the cavity region, OH-PLIF laser diagnostics was utilized to provide visualization of spanwise flame distribution. The laser sheet was directed normal to the core flow at three different locations, namely, the end of the cavity ramp, the cavity mid section, and immediately behind the cavity leading edge, as schematically illustrated in Fig. 13. The camera was positioned downstream looking upstream at an angle to capture the laser induced fluorescence signals within each plane of interest. The side wall of the combustor is located at the right of each image. The left edge of the obtained image extends just beyond the center-plane of the flowpath. The obtained image has a physical height of 1.75" and a physical width of slightly over 2". The instantaneous OH-PLIF flame image shows highly turbulent flamelet structures for all fueling conditions within each laser sheet plane (not shown). Therefore, average and standard deviation OH-PLIF images are shown in the present study to depict probability of flame spatial distribution.

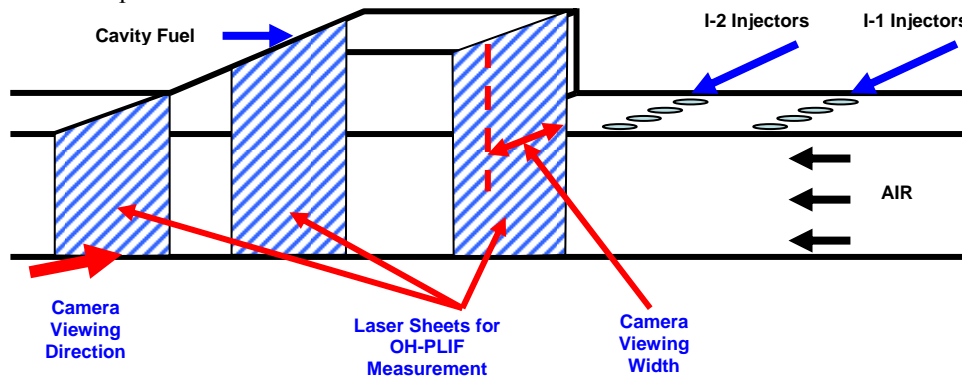


Figure 13. Schematic to illustrate the locations of laser sheet planes for OH-PLIF images and the orientation of the detecting camera. The flow is from right to left. The schematic is not to scale.

Figures 14(a) and 14(b) show the average and standard deviation OH-PLIF images, respectively, for a flame established with  $\phi = 0.8$  from the I-2 injectors and no cavity fueling. For the plane close to the cavity leading edge (right column in Fig. 14), it appears that there is flame distributed right behind the cavity step (average image) with unsteady flame randomly distributed within the thin shear layer and out of the cavity step along the side wall corner (standard deviation image). The flame spreading out of the cavity in Fig. 14 is very similar to the observed flame appearance in Fig. 9(b). Within this plane, there is no flame distributed around the in-board fuel plumes, which are invisible in OH-PLIF image, above the cavity volume. The combustion zone increases its size in both the mid and downstream laser sheet planes. Unfortunately, the quartz window cracked around the high-intensity combustion region due to intensive thermal shock during testing. Both attenuation of laser sheet intensity and scattering of the OH-PLIF signals from these window cracks can be easily seen at the mid-plane images in Fig. 14, indicating that the high-intensity combustion is mainly distributed in the rear half of the cavity. Comparing with those flame images with high cavity fuel flow rates in Figs. 4 and 6, where intensive combustion also mainly takes place in the rear half of the cavity volume, the fuel/air mixture within the cavity is projected to be relatively rich even without additional cavity fueling. Overall, flame is mainly distributed along the side wall for all three laser sheet planes.

Figure 15 demonstrates the flame distribution for combustor operating conditions identical to those in Fig. 14, except that a cavity fuel flow rate of 0.0043 lb/s was introduced. Comparing the upstream laser sheet plane in both Figs. 14 and 15, the introduction of additional cavity fuel creates less intensive combustion right behind the cavity step. Once again, comparing the observed flame structures from conditions with high cavity fuel flow rates in Figs. 4

and 6 with the OH-PLIF signal contours in Fig. 15 suggests that the mixture within the cavity is comparatively richer. Cracks on the window severely affect the OH-PLIF signals and, subsequently, prevent the drawing of further meaningful comparative conclusions as to the effects of additional cavity fueling on both cavity and main flame structures.

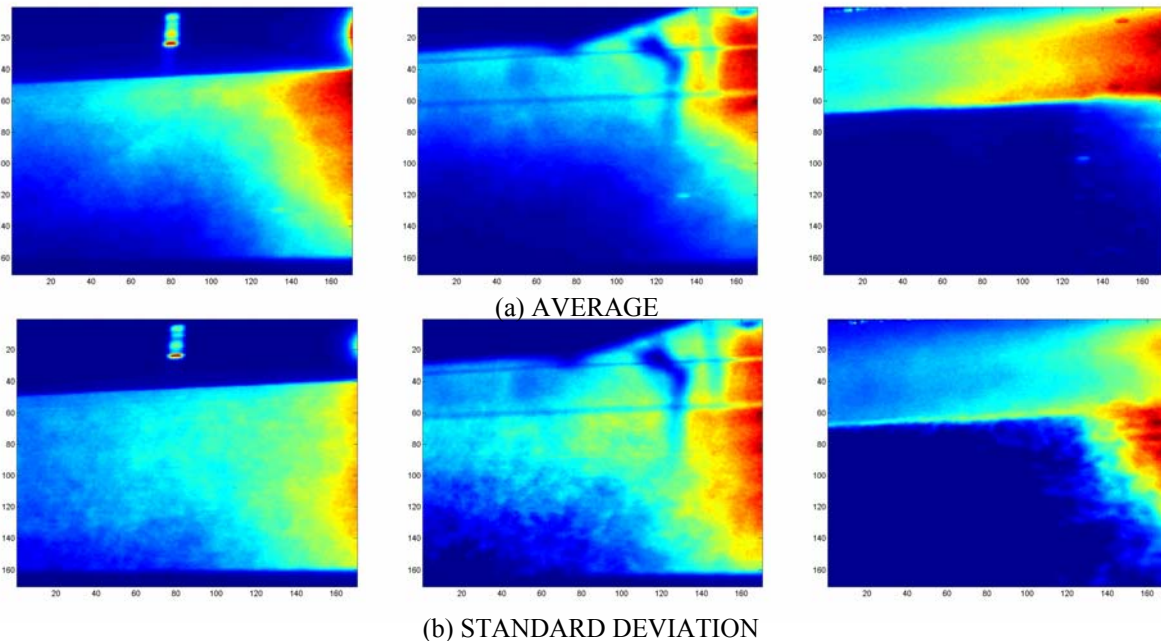


Figure 14. OH-PLIF images for flames around the cavity region without independent cavity fuel.  $M_{flight}=5.0$ ,  $q=500$  psf, I-2 injectors with  $\phi=0.8$ . Left column: end of cavity plane; middle column: cavity mid plane; right column: cavity leading edge plane. (a) Averaged flame images, (b) Standard deviation images.

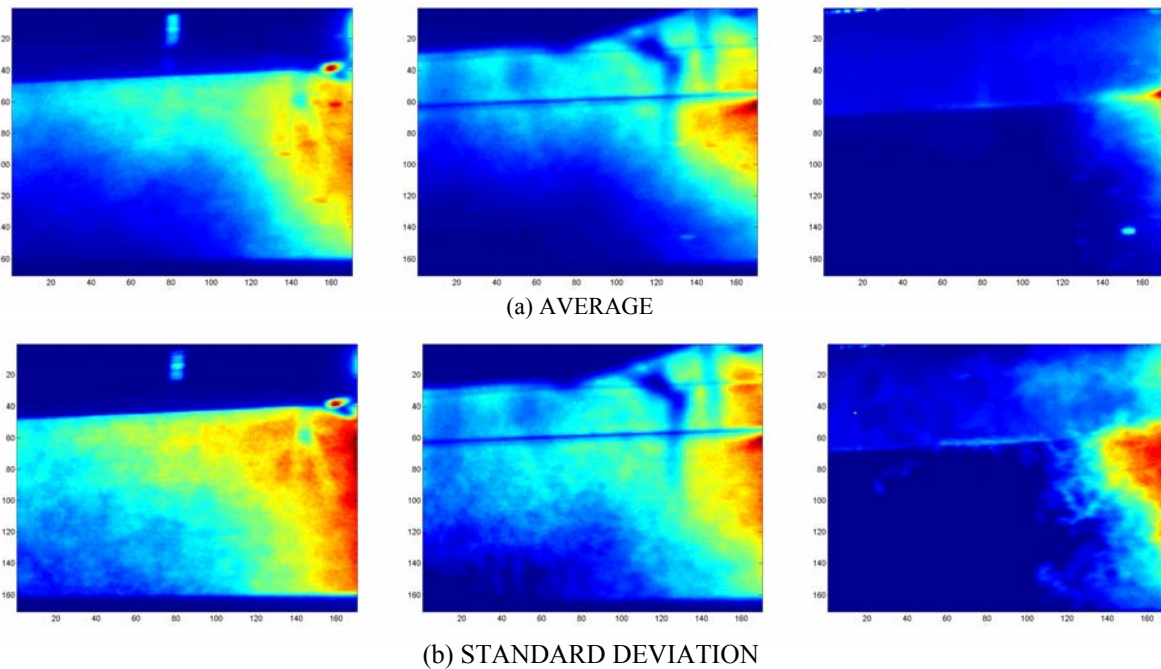


Figure 15. OH-PLIF images for flames around the cavity region with  $m_{pilot}=0.0043$  lb/s.  $M_{flight}=5.0$ ,  $q=500$  psf, I-2 injectors with  $\phi=0.8$ . Left column: end of cavity plane; middle column: cavity mid plane; right column: cavity leading edge plane. (a) Averaged flame images, (b) Standard deviation images.

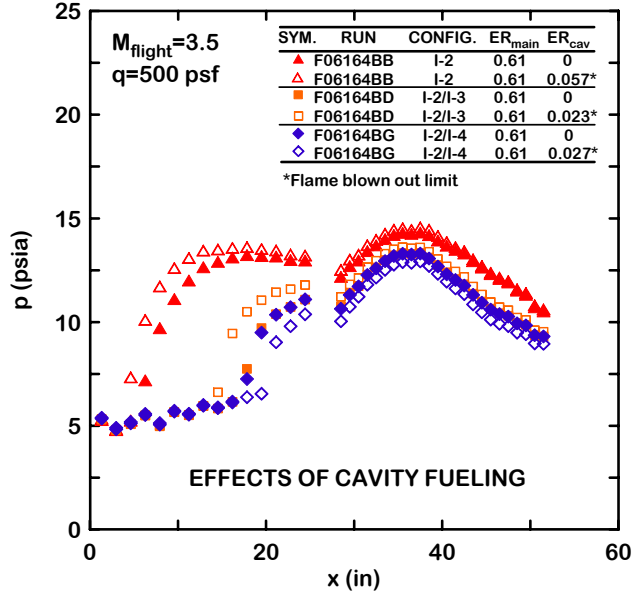


Figure 16. Wall static pressure profiles with and without separate cavity fueling with various fueling schemes for  $M_{flight}=3.5$  and  $q=500$  psf.

Figure 16 shows typical wall static pressure profiles inside a scramjet combustor with and without cavity fueling. It was found that the entire flame could be blown out by introducing a relatively small amount of fuel into the cavity for the present flowpath and injector designs. Only a small change to the wall static pressure profile can be observed before flame blowout in Fig. 16. Also tabulated in Fig. 16 are fuel equivalence ratios contributed by cavity fuel right before flame blowout. A very small increase in overall fuel equivalence can be achieved with additional cavity fuel. Meanwhile, the overall fuel equivalence ratio from the main fuel injector can be further increased to reach an unstart condition without flame blowout. Apparently, stabilization of the combustor flame and expansion of the combustor operability cannot be accomplished with cavity fueling, for the present flowpath and low-angle injection scheme. Fuel entrainment from the main fuel plumes of the present injector configuration alone is sufficient to maintain robust combustion inside the cavity and to facilitate the flame holding characteristics of the recessed cavity. Operation of independent cavity fueling should, therefore, be carried out with caution, since cavity rich blowout can be easily reached in the presence of main fuel plumes and can cause undesired consequences over the entire scramjet flowpath by destroying the flame holding capability of a cavity. The need to implement additional cavity fueling should be assessed with specific flowpath design and injection schemes.

Table 2. Composition of gas drawn from cavity base at various fueling conditions with  $M_{flight}=5.0$  and  $q=500$  psf.

Run	Configuration	ER(main)	ER(pilot)	O <sub>2</sub> (%)	NO(ppm)	NO <sub>2</sub> (ppm)	C <sub>x</sub> H <sub>y</sub> (%)
F06138AK	I-2	0.62	0.00	2.1	954	25	4.07
F06138AP	I-2	0.83	0.06	1.3	1144	14	2.42
F06138AP	I-2	0.83	0.00	2.1	1136	9	1.77
F06138AQ	I-2/I-3	0.68	0.06	2.0	803	18	3.10
F06138AR	I-2/I-3	0.82	0.06	1.5	728	7	2.93
F06143AF	I-2/I-4	0.63	0.00	0.4	771	9	1.38
F06143AH	I-2/I-4	0.79	0.07	0.9	755	3	2.46
F06143AI	I-2/I-4	1.01	0.08	1.3	961	12	2.71

#### Gas Composition within the Cavity

Composition of gas samples drawn from the cavity base close to the cavity leading edge are tabulated in Table 2 for some test conditions. The concentration of carbon monoxide was not included in Table 2 since its value is beyond the detection limit of the gas analyzer. The relatively low concentrations of oxygen and unburned hydrocarbons at dry basis indicate that the majority of the gas in this region is composed of combustion products, i.e., H<sub>2</sub>O, CO<sub>2</sub>, and probably CO. The oxygen concentration should be roughly three times the ethylene concentration to ensure stoichiometric combustion. The measured oxygen concentration in Table 2 clearly shows that if the detected

unburned hydrocarbon is assumed to be ethylene and no further reaction will take place for CO, there is insufficient oxygen to consume unburned hydrocarbons and CO locally for conditions with and without cavity fueling. In other words, gas mixtures within the cavity flame holder are already relatively rich in the present flowpath, in spite of the fact that combustion products constitute the majority of the gas mixture. Any fuel addition directly into the cavity will further enrich the cavity gas mixtures, since the oxygen has already been largely consumed. This explains why only a small amount of injection can be injected into the cavity before flame blowout for the present flowpath integrated with a low-angle injection scheme.

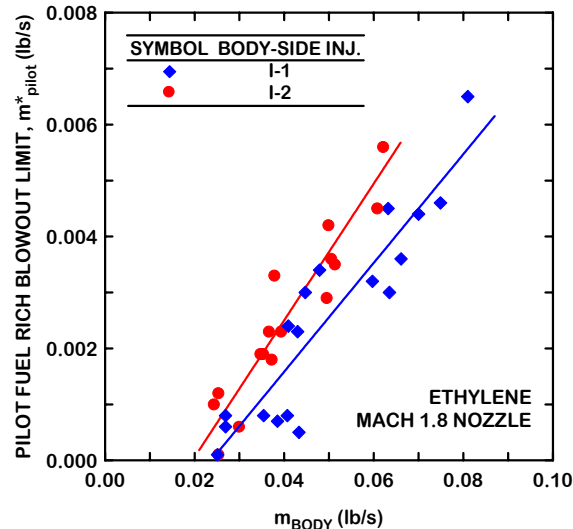


Figure 17. Relationship between pilot fuel rich blowout limit and fuel flow rate from body-side injection site for flight conditions simulated with the Mach 1.8 facility nozzle.

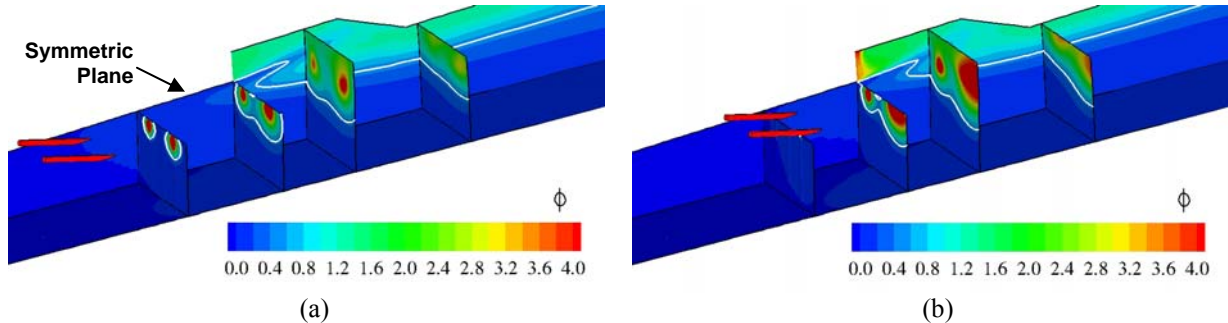


Figure 18. Fuel equivalence ratio contours from numerical calculations for  $M_{\text{flight}}=5.0$ ,  $q=500$  psf, and  $\phi=0.8$  using (a) I-1 injectors and (b) I-2 injectors. Flow is from left to right. Only half width of the combustor is shown.

#### Cavity Rich Blowout Limit with Main Fuel

Figure 17 shows the relationship between cavity fuel rich blowout limit (RBL) and body-side fuel flow rates for test conditions simulated with the Mach 1.8 facility nozzle. One of the observations is that the measured cavity RBL with main fuel flow in Fig. 17 is lower than that without main fuel flow. RBL of the pure cavity flame is beyond the flow meter capacity, as mentioned earlier. For the present flowpath, the use of flush-wall low-angle injectors on the body side can provide a wide range of fuel entrainment into the cavity for robust combustion. It was also found that the RBL correlates linearly with the body-side main fuel flow rate for the incoming air flow rates simulated by the Mach 1.8 nozzle. The effects of heated walls on flame stabilization, the short testing duration, and the rate of increase in cavity fuel flow all contribute to the observed uncertainties in identifying the cavity RBL. Based on Fig. 17, one can conclude that the fueling conditions with a high body-side main fuel flow rate, where fuel plumes can penetrate deeper into the core flow and thus may have less (more) fuel (air) entrainment into the cavity, can have a higher cavity fuel RBL. The same reasoning, however, cannot be applied to the observed difference between body-side fuel flow rates from I-1 and I-2 injectors. With a higher penetration height at the cavity leading edge for fuel plumes issuing from the upstream I-1 injectors, less fuel entrainment into the cavity and, thus, a higher RBL should

be expected for the conditions fueled with I-1 injectors. This expectation, however, is not confirmed by the observed trend in Fig. 17, probably due to the fact that the fuel plumes from I-1 injectors merge to create an aerodynamic blockage, preventing freestream air from being entrained into the cavity. Consequently, the required cavity fuel flow rate to reach RBL is reduced for the conditions fueled with I-2 injectors. To illustrate this phenomenon, Figs 18(a) and 18(b) show the numerical equivalence ratio contours for the present flowpath fueled with I-1 and I-2 injectors, respectively, at the same vitiator condition and fuel flow rate. The white line in Fig. 18 marks the location with a local  $\phi$  of 0.5. It is obvious that the fuel plumes from the I-1 injectors exhibit an extended degree of merging at the cavity leading edge plane in Fig. 18. More aerodynamic blockage from the I-1 fuel plumes, preventing air entrainment into the cavity is, therefore, expected.

Figure 19 shows that the measured RBL for flight conditions simulated with the Mach 2.2 facility nozzle is generally higher than that simulated with the Mach 1.8 nozzle using the I-1 injection site. This observation is in accord with the conclusion drawn from Fig. 10, where cavity operating limits increase with the characteristic air flow rate. Higher characteristic air flow rates are created for the conditions simulated with the Mach 2.2 facility nozzle. Therefore, slightly more cavity fuel can be added into the cavity before reaching RBL for a given cavity volume.

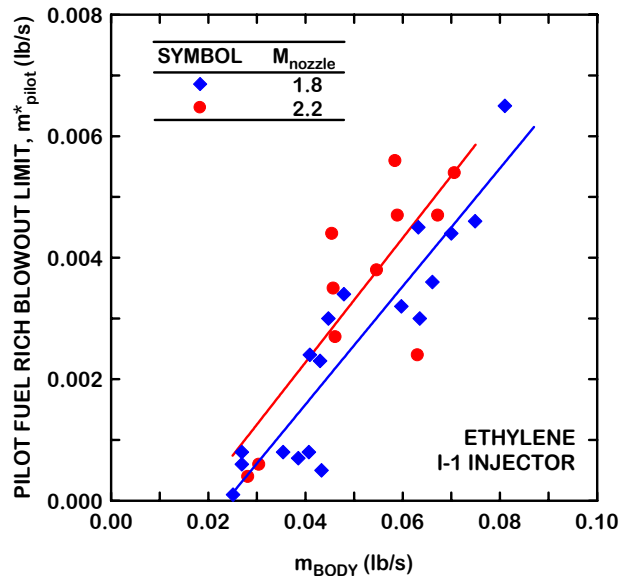


Figure 19. Relationship between pilot fuel rich blowout limit and fuel flow rate for I-1 injection site for flight conditions simulated with the Mach 1.8 and 2.2 facility nozzles.

### CONCLUSIONS

Flame structures and operating limits of a recessed cavity flame holder were investigated both experimentally and numerically, using a newly developed AFRL research scramjet flowpath at Wright-Patterson Air Force Base. This flowpath features a recessed cavity flame holder on the body wall and flush-wall low-angle injectors on both body and cowl walls. The recessed cavity features an array of independent fueling ports located at the aft cavity ramp. The flight conditions of interest were simulated with Mach 1.8 and 2.2 facility nozzles to cover Mach 3.5 to 5.0 flight conditions. Unheated ethylene was selected as the fuel for both main injector and independent cavity fueling ports. Shape, spatial distribution, and blowout limits of the cavity flames operated under various conditions were explored with numerical calculations and advanced diagnostics, including OH-PLIF imaging and high-speed video imaging. The cavity operating conditions include cavity fuel only, cavity fuel with a shock train established from air throttling, and main fuel with and without cavity fuel. The major conclusions of the present study are as follows:

1. With cavity fueling only, a significant variation in shape and spatial distribution of the cavity flame can be observed at various fuel flow rates. As the fuel flow rate increases, spatial distribution of the cavity flame changes from a location above the cavity base, to within a region reaching from the shear layer to the foot of the cavity ramp, and farther to along the cavity ramp. Within the operating limits of the cavity,

the size and structure of the main re-circulation zone inside the cavity remains the same for the present fueling port design.

2. With back pressurization to create a shock train upstream of a fueled cavity, the cavity flame becomes much more unsteady and exhibits significant differences from the cavity flame operated without back pressurization. Noticeably, a region containing yellow luminosity, probably from soot particles, appears in the frontal section of the cavity volume, as cavity fuel flow rate increases toward the rich blowout limit. At this condition, the flame was observed to spread out of the cavity volume, probably along the boundary layer on the combustor side walls.
3. For a fueled cavity with and without back pressurization, both the lean ignition limit and the lean blowout limit increase with the characteristic air flow rate. The measured lean blowout limit is lower than the lean ignition limit, probably due to the presence of hot combustion products and the effect of cavity wall temperature. The lean blowout limit is extended toward a lower value as the shock train is pushed upstream, due to changes in air entrainment characteristics as well as local temperature and pressure.
4. For a recessed cavity combined with main fuel injection, OH-PLIF images indicate that the additional cavity fueling eliminates the original flame distribution right behind the cavity backward-facing step. At this location, flame randomly extends out of the cavity volume along the side wall corners regardless of additional cavity fueling. No flame distributed within the in-board fuel plumes was observed at this location. For the present rectangular scramjet flowpath, the flame is mainly distributed within the body wall corners
5. The entire combustor flame can be easily blown out with a relatively small amount of additional cavity fuel for the present flowpath featuring a low-angle injection scheme. Qualitative composition analysis for gas sampled from the cavity base indicates that combustion products are the major gas species locally with a relatively rich oxygen/unburned hydrocarbon ratio. Consequently, injection of additional fuel into the cavity through the present cavity fueling ports increases the probability of blowing out the entire flame by disabling the flame holding capability of the recessed cavity.
6. The rich blowout limit for a cavity operated with both main and cavity fuel injections is lower than that for a cavity operated with cavity fuel alone, due to fuel entrainment from main fuel plumes. The rich blowout limit with main fuel injection was found to increase with the body-side fuel flow rate, due to reduced fuel entrainment into the cavity from deeply penetrating fuel plumes. Merging of fuel plumes injected from upstream injectors apparently creates an aerodynamic blockage for air entrainment into the cavity and, consequently, reduces the rich blowout limit.

#### ACKNOWLEDGEMENTS

This work was sponsored by the AFRL/Propulsion Directorate under contract number F33615-03-D-2326 (Contract monitor: Robert Behdadnia). Assistance from the air facility group of the Air Force Research Laboratory is acknowledged. Also, the authors would like to thank Paul Kennedy, Jack Barnett, (AFRL/PRAS), Matt Streby, and Steve Enneking (Taitech, Inc.) for their great assistance in rig operation, data acquisition, and hardware design and setup.

#### REFERENCES

1. Mathur, T., Gruber, M., Jackson, K., Donbar, J., Donaldson, W., Jackson, T., Billig, F., "Supersonic Combustion Experiments with a Cavity-Based Fuel Injector," *Journal of Propulsion and Power*, Vol. 17, No. 5, 2001, pp. 1305-1312.
2. Ben-Yakar, A. and Hanson, R., "Cavity Flame-Holders for Ignition and Flame Stabilization in Scramjets: An Overview," *Journal of Propulsion and Power*, Vol. 17, No. 4, 2001, pp. 869-877.
3. Yu, K., Wilson K., and Schadow, K., "Effect of Flame-Holding Cavities on Supersonic-Combustion Performance," *Journal of Propulsion and Power*, Vol. 17, No. 6, 2001, pp. 1287-1295.
4. Gruber, M., Baurle, R., Mathur, T., and Hsu, K.-Y., "Fundamental Studies of Cavity-Based Flameholder Concepts for Supersonic Combustors," *Journal of Propulsion and Power*, Vol. 17, No. 1, 2001, pp. 146-153.
5. Gruber, M., Donbar, J., Carter, C., and Hsu, K.-Y., "Mixing and Combustion Studies Using Cavity-Based Flameholders in a Supersonic Flow," *Journal of Propulsion and Power*, Vol. 20, No. 5, 2004, pp. 769-778.

6. Allen, W., King, P., Gruber, M., Carter, C., and Hsu, K.-Y., "Fuel-Air Injection Effects on Combustion in Cavity-based Flameholders in a Supersonic Flow," AIAA Paper 2005-4105, July 2005.
7. Rasmussen, C. C., Driscoll, J. F., Carter, C. D., and Hsu, K.-Y., "Characteristics of Cavity-Stabilized Fames in Supersonic Flow," *Journal of Propulsion and Power*, Vol. 21, No. 4, 2005, pp. 765-768.
8. Rasmussen C. C., Dhanuka, S. K., and Driscoll, J. F., "Visualization of Flameholding Mechanisms in a Supersonic Combustor Using PLIF," *Proceedings of the Thirty-First Symposium on Combustion*, The Combustion Institute, Pittsburgh, Vol. 31, pp. 2505-2512, 2007.
9. Rasmussen, C. C., Driscoll, J. F., Hsu, K.-Y., Donbar, J. M., Gruber, M. R., and Campbell, C. D., "Stability Limits of Cavity-Stabilized Fames in Supersonic flow," *Proceedings of the Thirtieth Symposium on Combustion*, The Combustion Institute, Pittsburgh, Vol. 30, pp. 2825-2833, 2005.
10. White, J. and Morrison, J. H., "A Pseudo-Temporal Multi-Grid Relaxation Scheme for Solving Navier-Stokes Equations," AIAA Paper 1999-3360, 1999.
11. <http://vulcan-cfd.larc.nasa.gov/>
12. Edwards, J.R., "A Low-Diffusion Flux-Splitting Scheme for Navier-Stokes Calculations," *Computers & Fluids*, Vol. 26, No. 6, 1997, pp. 635-659.
13. Menter, F.R., "Zonal Two Equation  $\kappa$ - $\omega$  Models for Aerodynamic Flows," AIAA Paper 1993-2906, 1993.
14. Wilcox, D. C., "Wall Matching, a Rational Alternative to Wall Functions," AIAA Paper 89-0611, 1989.
15. Baurle, R. A. and Eklund, D. R., "Analysis of Dual-Mode Hydrocarbon Scramjet Operation at Mach 4-6.5," *Journal of Propulsion and Power*, Vol. 18, pp. 990-1002, 2002.
16. Eklund, D. R., Baurle, R. A., and Gruber, M. R., "Computational Study of a Supersonic Combustor Fueled by an Aerodynamic Ramp Injector," AIAA Paper 2001-0379, 2001.
17. Singh, D. J. and Jachimowski, C. J., "Quasiglobal Reaction Model for Ethylene Combustion," *AIAA Journal.*, Vol. 32, No. 1, pp. 213-215, 1993.
18. Liu, J., Tam, C.-J., Lu, T., and Law, C. K., "Simulations of Cavity Stabilized Flames in Supersonic Flows Using Reduced Chemical Kinetic Mechanisms," AIAA Paper 2006-4862, July 2006.
19. Qin, Z., Lissianski, V. V., Yang, H., Gardiner, W. C., Davis, S. G., and Wang, H., *Proc. Combust. Inst.*, Vol. 28, pp. 1663-1669.